

Creation and Characterization of Lipid Nanoparticles Using Nanoparticle Tracking Analysis and Fluorescent Microscopy

Jonatan Haraldsson

jonhara@chalmers.se

Oscar Stommendal

oscarsto@chalmers.se

Abstract

In this experiment lipid nanoparticles (LNPs) were produced by varying methods and characterized with focus on their size and interaction with artificial lipid bilayers. Nano Tracking Analysis (NTA) revealed that production methods significantly influence LNP size. Using a higher PEG stabilizer concentration resulted in smaller particles, while the *Spark* mixing technique produced smaller and more uniform LNPs compared to manual or vortex mixing. Interestingly, a higher pH solvent unexpectedly led to smaller LNPs, contradicting theoretical predictions. However, the mRNA encapsulation efficiency under these conditions remains unknown and requires further investigation. Moreover, fluorescence microscopy showed that LNPs bound more effectively to lipid bilayers at lower pH, due to stronger electrostatic interactions. In summary, these findings emphasize the need for additional studies to assess mRNA content within LNPs and explore more lipid compositions to optimize LNPs for specific applications. Future work should continue focus on both nanoparticle formation and their effectiveness as carriers for mRNA delivery.

Keywords: *Nano Tracking Analysis, NTA, Lipid Nanoparticles, LNP, Lipid Bilayer, Fluorescent Microscopy.*

October 2024

Course: *Experimental Methods in Modern Physics, 3 hp*

Course Code: *TIF295*

Physics, MSc.

CHALMERS UNIVERSITY OF TECHNOLOGY



CHALMERS
UNIVERSITY OF TECHNOLOGY

1 Introduction

1.1 Background

Historically, humans have striven to live longer and healthier through medical advancements. By the end of the 18th century, the deadly disease smallpox ravaged the world. Edward Jenner, a British Physician, noticed that patients infected by cow pox later developed immunity towards smallpox [1]. From this, Jenner realized that protection against smallpox could be achieved by injecting patients with small amounts of cow-pox virus. Today, smallpox is considered eradicated thanks to Jenner's discovery [2], which was named *Vaccine* after the Latin word for cow, *Vacca*.

In addition to Jenner's vaccine, the recent COVID-19 pandemic is another example of how new vaccines can save lives. In this case, the vaccine contained mRNA encoded to produce antigens inside a cell [3]. For the mRNA to pass through cell membranes, it must be encapsulated in lipid-based nano-sized carrier particles, known as lipid nanoparticles (LNPs). In developing new treatments using mRNA, characteristics such as size and binding strength of the LNPs carriers are highly important.

In this experiment, sizes of LNPs, created under different conditions, were measured using nano tracking analysis (NTA). Furthermore, to simulate binding of the LNPs to a cell membrane, the binding to an artificially constructed lipid bilayer was studied using florescence microscopy.

1.2 Theory

Phospholipids – building blocks of cell membranes and LNPs, are molecules with water-attracting, hydrophilic tails and water-repelling, hydrophobic heads that can be connected in a lipid bilayer (see Figure 1) [4]. Moreover, the bilayer can occasionally bend into a sphere forming a liposome, as illustrated in Figure 1. In contrast to liposomes, LNPs have nucleotides (e.g. mRNA) in its center rather than an aqueous volume [5]. To encapsulate mRNA in LNPs, the pH is lowered in a solution of lipids and mRNA. This makes the heads of certain, ionizable lipids positively charged, attracting the negatively charged mRNA [6]. Subsequently, other lipids in the solution will, due to the hydrophobic effect gather around the “free” tails, forming nano particles.

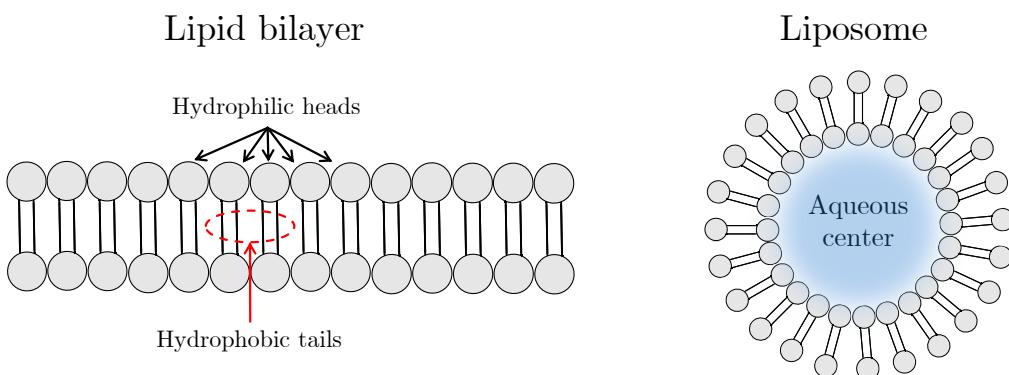


Figure 1: An illustration of a lipid bilayer and a liposome, which is a lipid bilayer bent into a spherical shape with an encapsulated volume.

When preparing lipid solutions, factors as mixing conditions, pH level and stabilizer concentration can affect LNP characteristics. PEG lipids are a common stabilizer, since they are believed bind to the surface of the LNPs during the self-assembly process [6]. Due to this, a higher concentration of stabilizers will increase the area-to-volume ratio of LNPs, which promotes smaller LNPs.

In a solution, LNPs undergo random, Brownian motion; a process related to particle size. Combining the Einstein relation for Brownian motion and Stokes' law, the hydrodynamic radius, R , for particles in a liquid with temperature T and viscosity η is given by

$$R = \frac{k_B T}{6\pi\eta D} = \left\{ D = \frac{1}{2t} \langle (x_0 - x(t))^2 \rangle \right\} = \frac{tk_B T}{3\pi\eta \langle (x_0 - x(t))^2 \rangle},$$

where $\langle (x_0 - x(t))^2 \rangle$ is the mean squared displacement (MSD) of particles during the time t . Hence, by tracking MSD, a distribution of radii can be obtained.

An additional method for studying small organic samples with high precision is through fluorescence microscopy. First, a fluorophore, i.e. a molecule that absorbs shortwave light at λ_a and emits light at $\lambda_e > \lambda_a$ (see Figure 2), is added to the sample [7]. Since the fluorophore has a unique $\Delta\lambda = \lambda_a - \lambda_e$ (Stoke shift), filters that block other wavelengths can be used to monitor the emitted light from fluorophores connected to specific particles in the sample.

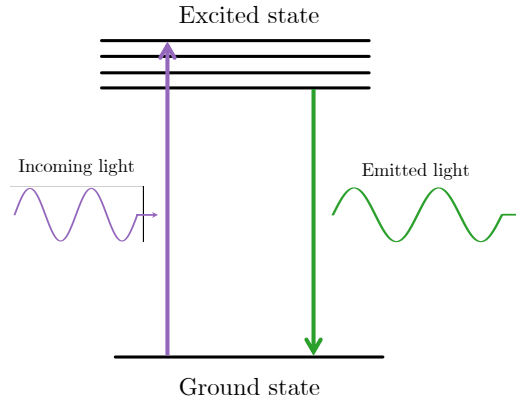


Figure 2: A schematic energy diagram that visualizes how incoming light is absorbed and then re-emitted at a longer wavelength, a process known as fluorescence.

2 Method

This section presents the experimental procedures used in the synthetization, size characterization, and imaging of lipid nanoparticles.

2.1 Synthesis of LNPs

Initially, five LNP sample solutions were synthesized using different types of mixing methods, as well as varying solvent pH and stabilizer volumes. Table 1 presents the main features of each sample.

Table 1: Overview of the samples synthesized during the first part of the experiment.

Sample	Solvent pH	Stabilizer	Mixing
1	4.0	Low	Manual
2	4.0	Low	Vortex
3	4.0	Low	SPARK
4	4.0	High	Vortex
5	7.4	Low	Vortex

Each solution was prepared similarly: first, a mRNA solution with a concentration of $c_2(\text{mRNA}) = 0.19 \text{ mg/mL}$ was prepared using 5x concentrated McIlvaine buffer (5xMB). The prepared buffers had $\text{pH}_L = 4.0$ and $\text{pH}_H = 7.4$. The dilution formula, $c_1V_1 = c_2V_2$ was used to get the correct proportions.

Subsequently, two lipid solutions were prepared, one containing a high amount of stabilizer (DMPE-PEG), and one with a lower amount. See Table 4 in Appendix B for the exact amounts. Since ethanol is volatile the *Eppendorf* tube used for mixing was closed between pipetting steps. Furthermore, the DSPC and cholesterol lipids are temperature sensitive and were put in a water bath at $T = 38.0^\circ\text{C}$.

The final samples were made by mixing the mRNA solution with the lipid solution, using either

- i) manual mixing (using the pipette),
- ii) vortex mixing ($\approx 20 \text{ s}$) or
- iii) *Spark*TM device (*NanoAssemblr*[®]) [8] .

For mixing method i) and ii), $40 \mu\text{L}$ of lipid solution was pipetted to an *Eppendorf* tube. Then, $120 \mu\text{L}$ of mRNA solution was added quickly, followed by mixing. Lastly, $160 \mu\text{L}$ of 5xMB with pH_H was added. Using *Spark* mixing, all components were pipetted to separate “wells” in a designated container used with the *Spark* instrument [8]. After mixing, the solution was pipetted back to a fresh *Eppendorf* tube.

2.2 Size Characterization of LNPs using NTA

The size of the LNPs was determined using a nanoparticle tracking analysis (NTA) device (*NanoSight*). Each sample in Table 1 was diluted 1 000x with 5xMB (pH_H), except for solution 3, which was diluted 5 000x. The dilution was made to increase result accuracy, as the NTA performs better at lower particle concentrations. Subsequently, a small syringe was used to insert sample solution to the NTA device, which was set to measure (track) every 2 seconds. Each sample was measured for 5 minutes, where new sample solution was inserted every minute. Between each measurement the device was flushed by rinsing the tubing, first with degassed (to remove air and other particles, which can interfere with the tracking analysis) ultrapure water and then with 5xMB (pH_H). The resulting data was analyzed using `python`, and a histogram with a log-normal fit for the LNP size distribution was generated for each sample.

2.3 Estimation of LNP Binding to a Lipid Bilayer

To simulate binding of LNPs to a cell membrane, the number of LNPs that bound to an artificial lipid bilayer was estimated using fluorescent microscopy. The set-up, provided schematically in Figure 3, contained a chip with channels and a hydrophilic glass plate attached to the bottom, a container and tubing to a syringe. To obtain a hydrophilic glass plate, an ozone treatment, described in Appendix C, was done. The syringe was controlled via an electronic pump.

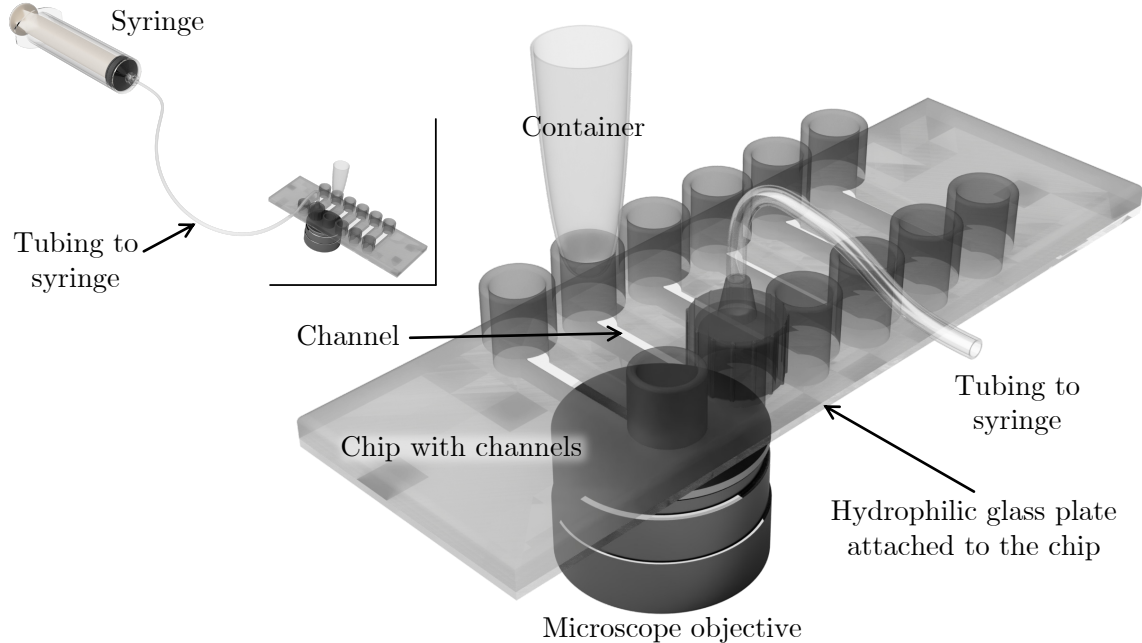


Figure 3: 3D schematic of the set-up in the fluorescent microscope. The overview Figure in the upper left shows how the set-up was connected to the syringe. In the main Figure in the center shows a model of the chip with channels, the container and the syringe tubes. At the bottom of the chip, a hydrophilic glass plate is attached. The microscope objective was placed below the channel. The 3D model of the syringe was obtained through the *McMaster-Carr* plugin in Autodesk Fusion [9].

The lipid bilayer was constructed by pumping a solution with lipid vesicles (liposomes) from the container to the syringe via the channel. The hydrophilic glass plate attracted the vesicles, where they ruptured and unfolded, forming a single bilayer. When the channel was rinsed, deionized LNP solutions, prepared according to Table 2, were pumped over the bilayer until saturation, i.e. when the number of bound particles no longer increased. During pumping, microscope images were captured and rendered into a movie, later used to estimate bilayer binding with a provided MATLAB script.

Table 2: Features of the LNP solutions that were used to estimate binding.

Run	Mixing	Solvent pH	Dilution
1	<i>Spark</i>	7.4	100x
2	<i>Spark</i>	4.0	100x

3 Results and Discussion

This section presents the size distributions of LNPs measured using NTA, followed by an analysis of their binding behavior to lipid bilayers using fluorescence microscopy. Theoretical insights and potential sources of error are discussed in relation to experimental conditions.

3.1 Size Characterization of LNPs using NTA

Figures 4a, 4b and 4c show the LNP size distributions with different mixing conditions. The black line is a fitted log-normal curve and the orange vertical lines denotes the fit mean and standard deviation, generated through python. Note that the standard deviation marker in the Figures marks the point for $\mu + \sigma$, though the value displayed is the value for σ .

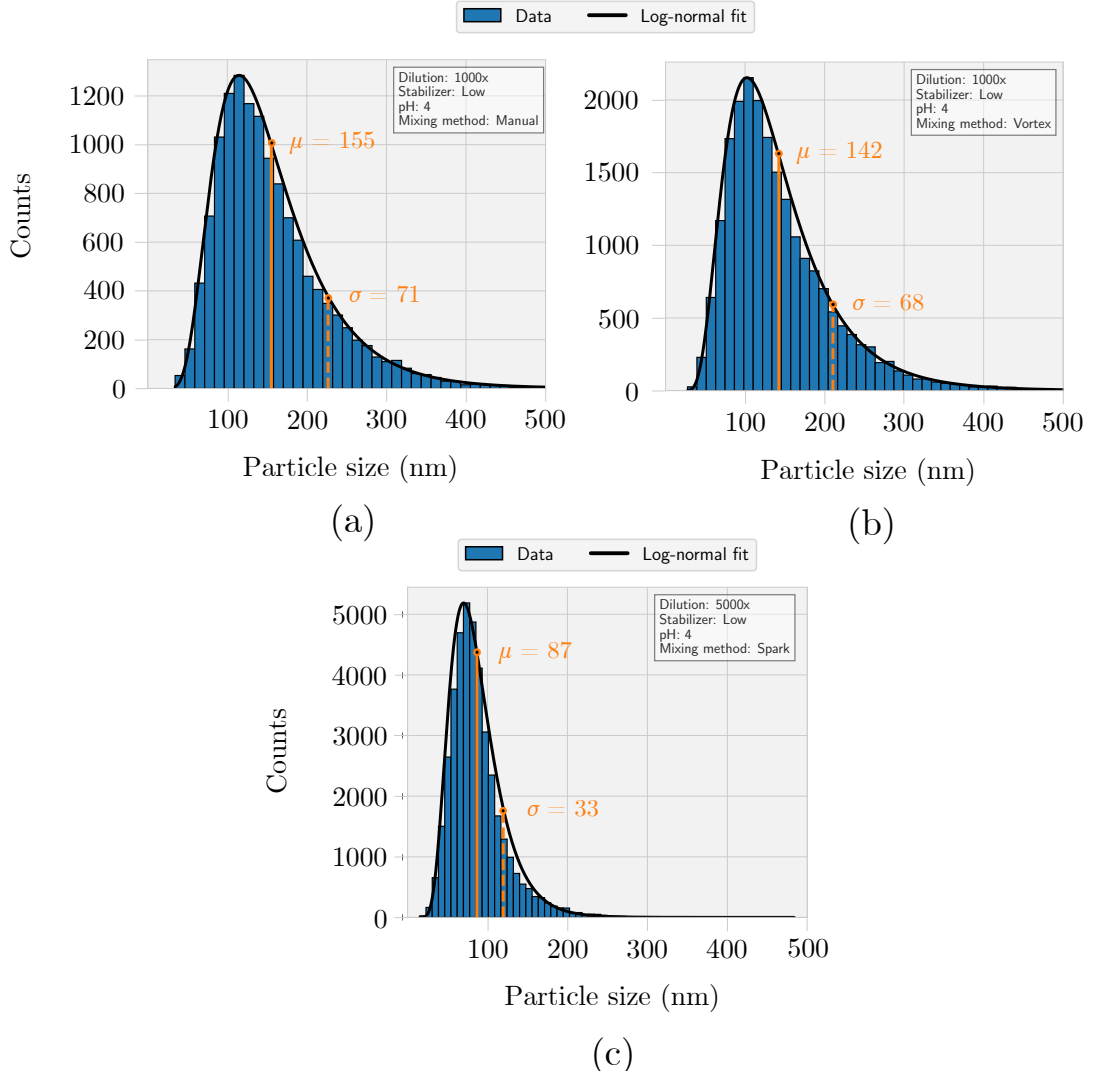


Figure 4: Three LNP size distributions originating from different mixing conditions – manual (a), vortex (b) and *Spark* (c) mixing. The black and orange lines follow from a log-normal fit. The *Spark* mixing had both lowest mean and standard deviation followed by Vortex mixing.

It follows that a more sophisticated mixing procedure, in this case *Spark* (Figure 4c), provides smaller and more consistently sized LNPs. Similarly, if manual and vortex mixing are compared (Figures 4a and 4b), the vortex mixing tends to give slightly smaller particles with less deviation. In addition, the *Spark* mixing is an automatic procedure and should, hence, be more repetitive in producing a similar result every time. Furthermore, the arise of a log-normal distribution is typical when studying particle size distributions, as also found by [10] and [11]. Although the mission of explaining why this is the case seems rather unexplored.

Secondly, Figures 5a and 5b, show the LNP size distributions with different pH in the buffers along with a log-normal fit mean and standard deviation. In this case, data suggests that pH_H corresponds to slightly smaller particles and a narrower distribution. Considering that a lower pH together with the ionizable lipids trigger the self-assembly of LNPs, a low-pH solution should favor the formation of LNPs. However, since the NTA only measures particle size and quantity, and hence not mRNA within the observed particles, the quality of the observed particles is unknown. Put differently, lipid particles are formed in the pH_H solution, however, in theory they should contain less-to-none mRNA, which consequently makes them non-suitable as nano carriers. Again, to measure the mRNA content in the observed particles, additional tools and further investigations are required.

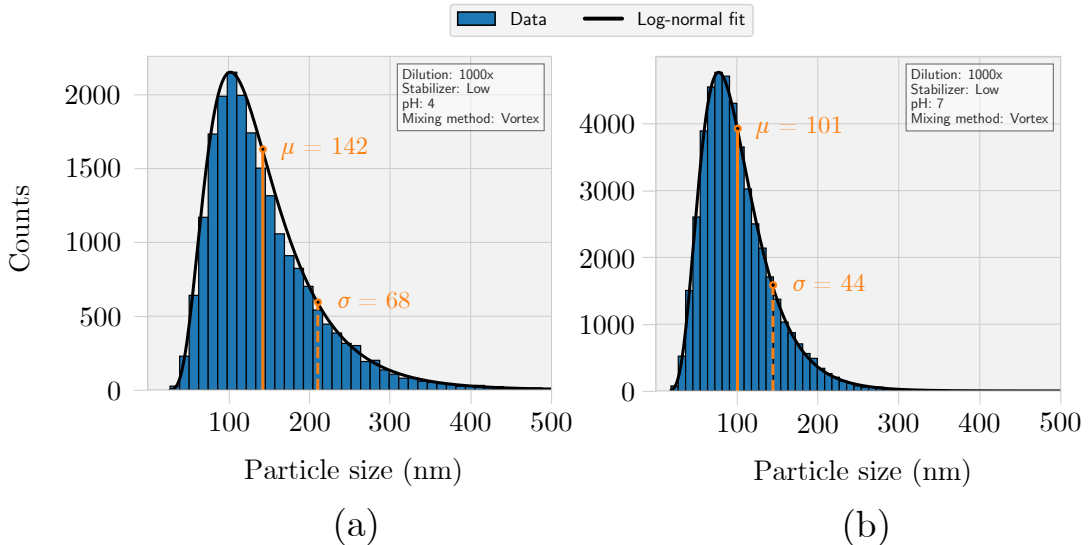


Figure 5: Two LNP size distributions with different pH in the buffers, pH_L (a) and pH_H (b). The black and orange lines follow from a log-normal fit. Note that the marker for σ is actually the marker for $\mu + \sigma$, though the value displayed is that for σ .

Thirdly, Figures 6a and 6b, show the LNP size distributions with different stabilizer concentrations, again with a log-normal fit, mean and standard deviation. According to the Figure, high stabilizer concentration seems to promote the formation of smaller LNPs with less standard deviation. The stabilizer concentrations differ by a factor of 8 in % mol (see Table 4 in Appendix B), which in this case corresponds to a mean particle size difference of $142 - 88 \text{ nm} = 54 \text{ nm}$. This result confirms that stabilizers (PEG lipids) can be added with the purpose of reducing size of LNPs [6].

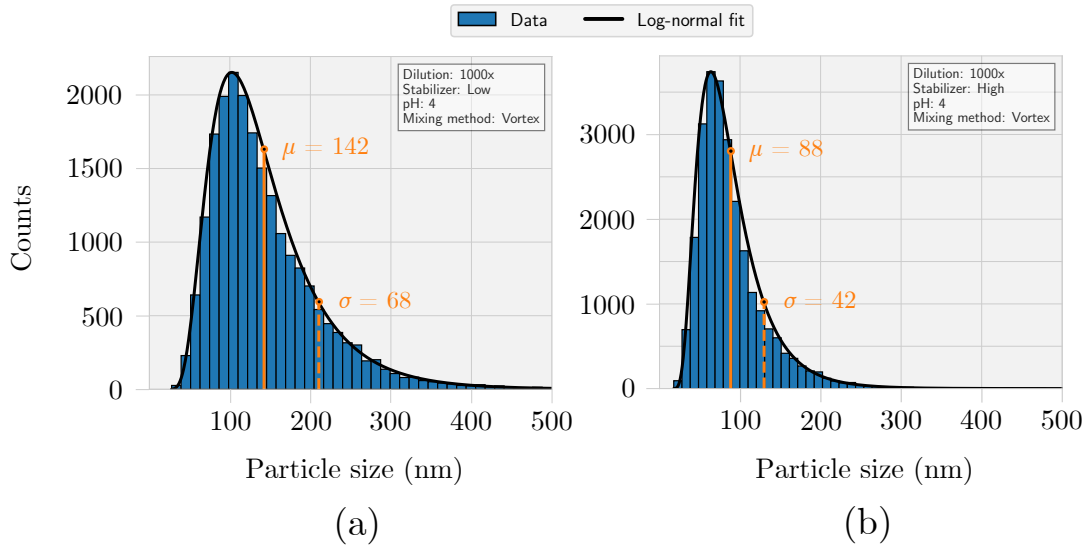


Figure 6: Two LNP size distributions with different stabilizer concentrations, low (a) and high (b). The black and orange lines follow from a log-normal fit. Note that the marker for σ is actually the marker for $\mu + \sigma$, though the value displayed is that for σ .

In summary, the complete set of all samples, along with mean and standard deviation of the log-normal fit are available in Table 3. The experiment in general had a somewhat qualitative nature, where the definition of a “good” result was not clearly defined. However, some observations and comments can be made regarding the reliability in the results. In medicine applications, particle size plays a large role [12]. For example, [13] found that particles less than ~ 10 nm in size may be rapidly eliminated by the kidneys, whereas particles larger than 200 nm might be removed directly from the blood stream. In this sense, sample 3 and 4 in Table 3 are most preferable.

This implies that developers of LNPs for medical purposes, should aim to achieve a narrow size distribution with a well-defined mean. Furthermore, ensuring that the majority of the LNPs fall within the optimal size range, maximizing their effectiveness for their specific application. As found in this experiment, stabilizer lipids and mixing conditions can play an important role in controlling the size of LNPs. By adjusting these parameters, developers can influence the size distribution of LNPs, allowing customization to meet the specific requirements of their intended application.

Moreover, [12] also emphasizes the importance of possible methods for measuring the encapsulation in LNPs. This is linked to the discussion on varying the buffer pH in the LNPs solution. Without such methods, one could assume that the high pH solution gives “better” LNPs.

Lastly, note that sample 2 has served as a reference throughout the discussion above, as it appears in every comparison when varying mixing condition, pH and stabilizer concentration. This means that any potential errors in the preparation or analysis of this sample would propagate through the comparative analysis, affecting the overall conclusions. Since each sample was carefully prepared according to the experimental instructions, the risk of such errors should be minimized. To evaluate the consistency within the method, a comparison of similar samples are required.

Table 3: Main features of each test sample along with the found mean and standard deviation of the size distributions. The latter were generated through a log-normal fit using python.

Sample	pH	$V_{\text{stabilizer}}$	Mixing	Mean [nm]	Std [nm]	% std
1	4	Low	Manual	155	71	46
2	4	Low	Vortex	142	68	48
3	4	Low	<i>Spark</i>	87	33	38
4	4	High	Vortex	88	42	47
5	7.4	Low	Vortex	101	44	44

3.2 Estimation of LNP Binding to a Lipid Bilayer

The number of detected particles per frame, captured every 2s during the formation of the lipid bilayer is given in Figure 7. Up until frame ~ 200 , there is a steady increase in the amount of detected lipid vesicles attached to the glass plate (see Figure 3). After frame 200 a significant drop occurs, which indicate that the vesicles are rupturing and unfolding into a flat bilayer. However, as the number of particles does not drop to zero, it is possible that not all vesicles have unfolded, thus, forming an incomplete layer. The slight increase of particles seen after the drop, may also be due to the incomplete bilayer still attracting vesicles.

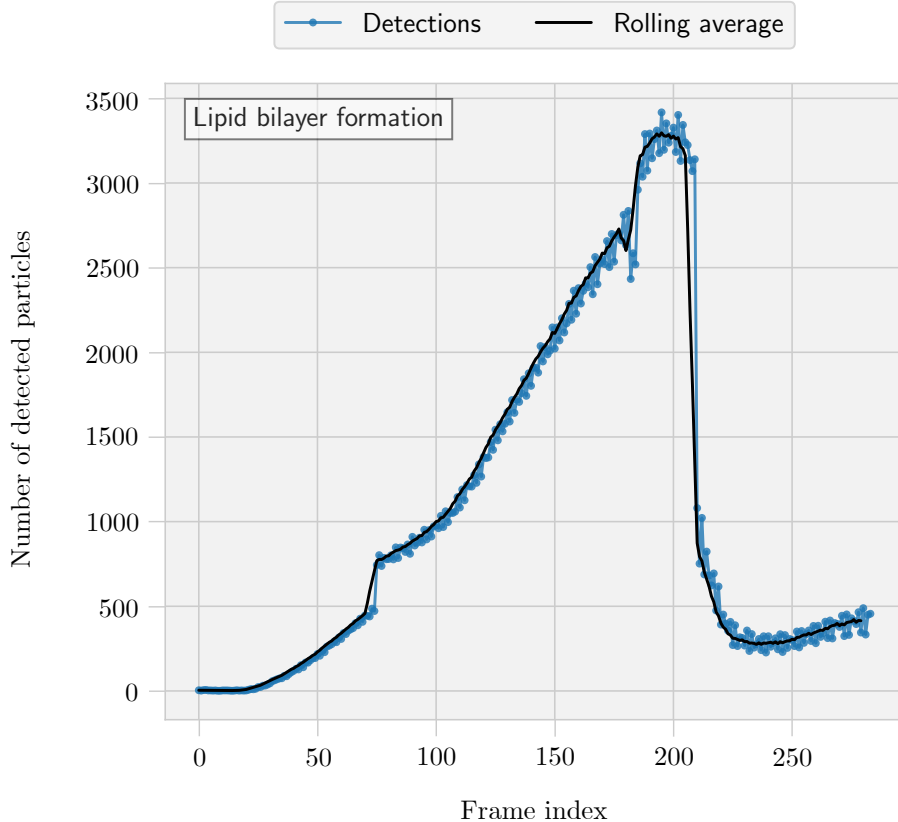


Figure 7: Detected particles per frame while forming the lipid bilayer, where the black line is the rolling average. Each frame corresponds to 2s.

In Figure 8 the number of detected LNPs bound to the bilayer in each frame are given for the two different solutions. The detected number of particles indicate that the solution with lower pH allow more LNPs to bind, which could be linked to the slightly negatively charged bilayer. Since an acidic solution in general has a surplus of H^+ ions, the solution, and hence the LNPs, should experience a stronger electrostatic attraction to the negatively charged bilayer. Instead of electrostatic attraction, protein bindings such as Neutravidin-biotin can be used to attract LNPs to a bilayer in pH7 [14].

As more LNPs bind to the bilayer, the structure may gradually become more disintegrated, obstructing the binding process. Although the solution with higher pH was run first, the possible disintegration caused to the bilayer during this run, did not seem to affect the stronger binding of the pH4 solution.

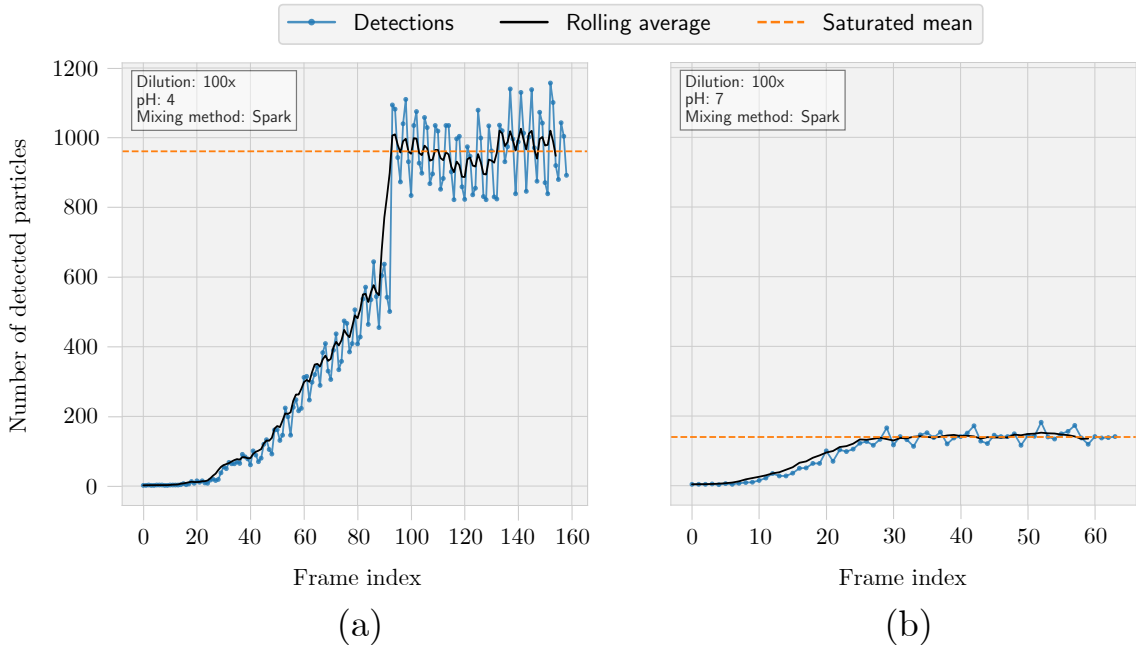


Figure 8: Number of detected particles per frame for the sample with low (a) and high (b) pH. The black line denote a rolling average and the orange line is the mean of the number of detections when the binding to the bilayer has saturated.

4 Conclusions

In this work, size of lipid nanoparticles (LNPs) produced by slightly different methods was measured using Nano Tracking Analysis (NTA). In addition, a fluorescent microscope was utilized to investigate the binding of LNPs to an artificial lipid bilayer, simulating LNP interactions with cell membranes.

To begin, the different methods for synthesizing LNPs clearly has an effect on the LNP characteristics. For instance, as hypothesized by [6], using a higher concentration of PEG lipids results in smaller particles. In addition, more sophisticated mixing methods, in this case *Spark*, provides some advantages such as smaller LNPs with less deviation and possibly a more repetitive result. Contrary to theoretical expecta-

tions, a higher pH solvent resulted in smaller particles and narrower size distributions. However, since NTA measures particle size and concentration without assessing the mRNA content within LNPs, the quality of these particles remains unclear. Higher pH conditions may lead to LNPs with low mRNA content, making them unsuitable as nano-carriers. In summary, varying stabilizer concentration and mixing method, developers can customize the characteristics of LNPs to fit their certain application.

When estimating the binding of LNPs to a cell membrane, LNPs bound more effectively to an artificial lipid bilayer when present in a solution with lower pH levels. This is likely due to the stronger electrostatic interactions between the negatively charged bilayer and the more acidic LNP solution.

In conclusion, these results highlight areas for further investigation, such as additional techniques to examine the mRNA content within LNPs in solutions with different pH. This will help determine not only the formation of nanoparticles but also their viability as effective mRNA carriers. Additionally, exploring a wider variety of lipid compositions could provide further insight into optimizing LNP for specific applications. More research in this area could unlock the full potential of LNPs, paving the way for more effective mRNA therapies that could greatly impact modern medicine, and perhaps save us from the next pandemic.

References

- [1] E. Jenner, “An inquiry into the causes and effects of the variolæ vaccinæ”, in London: Sampson Low, 1798. [Online]. Available: <https://www.jameslindlibrary.org/jenner-e-1798/>.
- [2] U.S. Centers for Disease and Control and Prevention CDC. “History of smallpox”. (2024), [Online]. Available: <https://www.cdc.gov/smallpox/history/history.html> (visited on 15/10/2024).
- [3] G. Karlsson Hedestam and R. Sandberg, *The nobel prize in physiology or medicine 2023*, 2023. [Online]. Available: <https://www.nobelprize.org/prizes/medicine/2023/advanced-information/> (visited on 04/10/2024).
- [4] B. Alberts, A. Johnson, J. Lewis *et al.*, “Molecular biology of the cell”, in 4th. New York: Taylor & Francis Inc., 2002, ch. Chapter 10, ISBN: 9780815340720. [Online]. Available: <https://www.ncbi.nlm.nih.gov/books/NBK26871/>.
- [5] J. Natarajan. “Lnps vs conventional liposomes”. (), [Online]. Available: <https://healthcare.evonik.com/en/news-and-events/blog/lnps-vs-conventional-liposomes-222475.html> (visited on 16/10/2024).
- [6] C. Hald Albertsen, J. A. Kulkarni, D. Witzigmann, M. Lind, K. Petersson and J. B. Simonsen, “The role of lipid components in lipid nanoparticles for vaccines and gene therapy”, *Advanced Drug Delivery Reviews*, vol. 188, p. 114 416, 2022, ISSN: 0169-409X. DOI: <https://doi.org/10.1016/j.addr.2022.114416>. [Online]. Available: <https://www.sciencedirect.com/science/article/pii/S0169409X22003064>.
- [7] J. Lakowicz, “Principles of fluorescence spectroscopy”, in Springer, Jan. 2006, vol. 1, ch. 1, ISBN: 978-0-387-31278-1. DOI: [10.1007/978-0-387-46312-4](https://doi.org/10.1007/978-0-387-46312-4).
- [8] Precision Nano Systems, *Nanoassembler® spark™*, 2022. [Online]. Available: <https://www.precisionnanosystems.com/docs/default-source/pni-files/brochures/spark-brochure.pdf> (visited on 15/10/2024).
- [9] McMaster, *Plastic syringe with luer slip connection, clear, 80 ml capacity*. [Online]. Available: <https://www.mcmaster.com/7510A36/> (visited on 14/10/2024).
- [10] L. Kiss, J. Söderlund, G. Niklasson and C. Granqvist, “The real origin of lognormal size distributions of nanoparticles in vapor growth processes”, *Nanostructured Materials*, vol. 12, no. 1, pp. 327–332, 1999, ISSN: 0965-9773. DOI: [https://doi.org/10.1016/S0965-9773\(99\)00128-2](https://doi.org/10.1016/S0965-9773(99)00128-2). [Online]. Available: <https://www.sciencedirect.com/science/article/pii/S0965977399001282>.
- [11] E. Limpert, W. A. Stahel and M. Abbt, “Log-normal Distributions across the Sciences”, *BioScience*, vol. 51, no. 5, pp. 341–352, May 2001, ISSN: 0006-3568. DOI: [10.1641/0006-3568\(2001\)051\[0341:LNDATS\]2.0.CO;2](https://doi.org/10.1641/0006-3568(2001)051[0341:LNDATS]2.0.CO;2). eprint: <https://academic.oup.com/bioscience/article-pdf/51/5/341/26891292/51-5341.pdf>. [Online]. Available: [https://doi.org/10.1641/0006-3568\(2001\)051%5B0341:LNDATS%5D2.0.CO;2](https://doi.org/10.1641/0006-3568(2001)051%5B0341:LNDATS%5D2.0.CO;2).

- [12] C. Chen, C. Chen, Y. Li, R. Gu and X. Yan, “Characterization of lipid-based nanomedicines at the single-particle level”, *Fundamental Research*, vol. 3, no. 4, pp. 488–504, 2023, ISSN: 2667-3258. DOI: <https://doi.org/10.1016/j.fmre.2022.09.011>. [Online]. Available: <https://www.sciencedirect.com/science/article/pii/S2667325822003764>.
- [13] N. Hoshyar, S. Gray, H. Han and G. Bao, “The effect of nanoparticle size on in vivo pharmacokinetics and cellular interaction”, *Nanomedicine*, vol. 11, Mar. 2016. DOI: <10.2217/nnm.16.5>.
- [14] I. Menon, M. Zaroudi, Y. Zhang, E. Aisenbrey and L. Hui, “Fabrication of active targeting lipid nanoparticles: Challenges and perspectives”, *Materials Today Advances*, vol. 16, p. 100299, 2022, ISSN: 2590-0498. DOI: <https://doi.org/10.1016/j.mtadv.2022.100299>. [Online]. Available: <https://www.sciencedirect.com/science/article/pii/S2590049822000959>.
- [15] H. X. Nguyen and C. N. Nguyen, “Microneedle-mediated transdermal delivery of biopharmaceuticals”, *Pharmaceutics*, vol. 15, no. 1, 2023, ISSN: 1999-4923. DOI: <10.3390/pharmaceutics15010277>. [Online]. Available: <https://www.mdpi.com/1999-4923/15/1/277>.
- [16] J. H. Jung and S. G. Jin, “Microneedle for transdermal drug delivery: Current trends and fabrication”, *Journal of Pharmaceutical Investigation*, vol. 51, no. 5, pp. 503–517, 2021. DOI: <10.1007/s40005-021-00512-4>. [Online]. Available: <https://doi.org/10.1007/s40005-021-00512-4>.
- [17] Method of making coated microstructures, by H.S. Gill, M.R. Prausnitz. (2014 June 14). US9364426B2 [Online]. Available: <https://patents.google.com/patent/US9364426B2/en>.
- [18] Wikipedia. “Ozone layer”. (), [Online]. Available: https://en.wikipedia.org/wiki/Ozone_layer (visited on 17/10/2024).

Appendix

A An Invention Enabled by Fluorescent Microscopy

A common method for drug delivery into the body, especially for delivering vaccines, is direct injection to the blood stream using a hypodermal needle attached to a syringe. However, treatments with this method have some disadvantages. Firstly, it requires trained personnel to ensure the drug is properly injected, and secondly, it is often a painful and perhaps scary process. An alternative way to inject medicine, first patented in 1976 [15], is through transdermal microneedles, e.g. a small patch with needles ($150 - 1500 \mu\text{m}$ in length and $1-25 \mu\text{m}$ in tip thickness) that only penetrate the upper layers of the skin [16].

To improve the dissolving of drugs after the microneedles have been inserted into tissue, coatings are sometimes applied to the needles prior to use [16]. If solid microneedles are used, the needles can be coated with the drug itself. To conveniently apply coating, a device and methods that can be used for coating various types of microneedles in different shapes and sizes was patented by Gill and Prausnitz [17].

In some steps described in [17], a fluorescence microscope was used. For instance, after the needles were coated and inserted into tissue, images from fluorescence microscopy was used to check for residual coating. Residual coating could give an indication or correspond to how much of the coating that actually went into the tissue. Furthermore, fluorescent microscopy images were also used to verify that the applied coating was distributed uniformly across the microneedle. In conclusion, the use of fluorescence microscopy played a central role in the realization of the patent, as it enabled them to verify the method of coating microneedles.

As described above, the first microneedle was patented in 1976. However, the invention and corresponding patent presented by Gill and Prausnitz was obviously considered a new invention – sufficiently different from previous patents in the area [17]. The claims made by Gill and Prausnitz that provided the basis for approving the patent are summarized below.

1. The only independent claim describes a step-by-step method for coating at least one microneedle. It includes details on how the coating is prepared and how the “physical mask” – used to coat the needle fits the coating process.
2. The rest of the claims are dependent, essentially providing a more detailed description of the method, such as specific configurations of the physical mask, variations in the coating liquid, and different materials for the microneedles.

B Lipid Solution Configurations

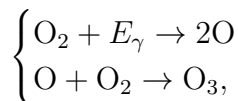
Table 4 below shows the components used in each stabilizer solution during the synthesis of LNPs. Samples from these solutions were mixed with the mRNA solution in order to create the final LNP-mRNA complexes.

Table 4: The lipid configurations in each type of stabilizer solution during the synthetization of LNPs. The component DMPE-PEG denotes the actual stabilizer. Note also that ethanol was only used as a solvent.

Stabilizer type	High Stabilizer		Low Stabilizer	
Component	Volume (μL)	% mol	Volume (μL)	% mol
MC3	7.71	50	7.71	50
DSPC	3.79	10	3.79	10
Cholesterol	6.62	36	7.27	39
DMPE-PEG	21.39	4	2.67	0.5
DSPE-PEG Biotin	4.34	0.03	4.34	0.03
NBD-DOPE	2.66	0.3	2.66	0.3
Ethanol	1.49	Solvent	19.55	Solvent

C Ozone Treatment

To ensure a hydrophilic surface that would attract liposomes in the solution and promote the formation of a lipid bilayer, the glass plate attached to the bottom of the chip was thoroughly cleaned. After cleaning the plate with ultrapure water and ethanol the glass plate was put in an ozone cleaner. The ozone cleaner uses, similar to what's happening in the ozone layer [18], UV radiation to form ozone according to



where E_γ is the energy from a UV photon γ . Since ozone is highly reactive, it reacts to the silica in the glass, making it more negatively charged. The negatively charged plate has accordingly a higher wettability or hydrophilicity. To display the difference before and after the ozone treatment, Figure 1 contains one treated (left) and one non-treated glass plate (right), both with an identical volume of water dropped. The figure shows that there is a significant difference in wettability before and after treatment.

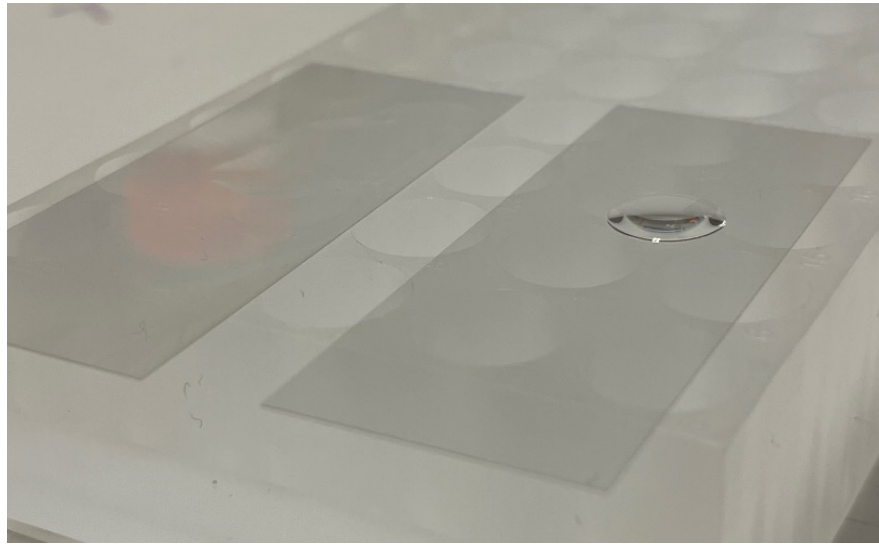


Figure 1: Two identical glass plates, where an identically size droplet of water added on top. The left plate has been ozone treated, while the right has not.

D Other Results

Figures 2 and 3 below illustrate the formation of the lipid bilayer in two ways. Figure 2 shows snapshots of frames 1, 44, 205 and 225 during the fluorescent microscopy, while Figure 3 shows the number of detections as a function of frame number. Notice the formation in the start, case (a) – (c) in Figure 2 or the increasing phase in Figure 3, where the bilayer is constructed. The sudden decrease of particles then visualized is a consequence of the eruption of the lipids, where the lipid construction collapses. This corresponds to case (c) – (d) in Figure 2 and the sudden drop in Figure 3.

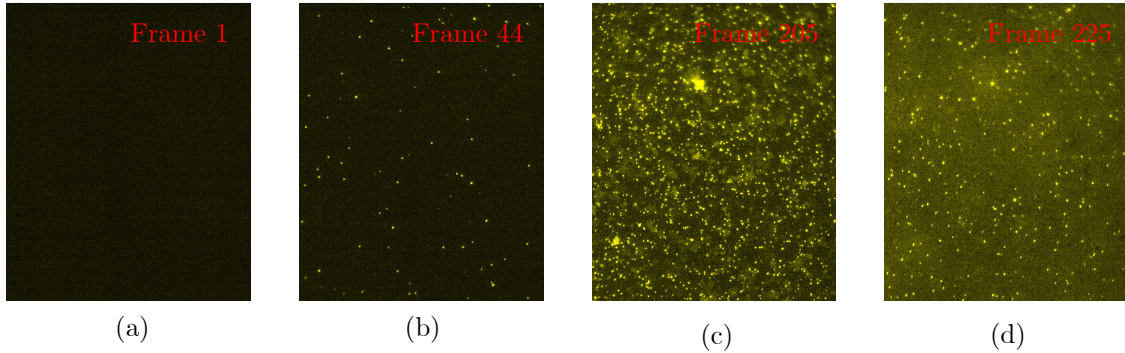


Figure 2: Snapshots from frames 1 (a), 44 (b), 205 (c) and 225 (d) during the formation of the lipid bilayer. Compare this to the graph in Figure 3 below, which shows the number of detections as a function of frame number. Note the significant decrease in particles between (c) and (d). This is a direct consequence of the eruption of the lipid bilayer, as explained in the text.

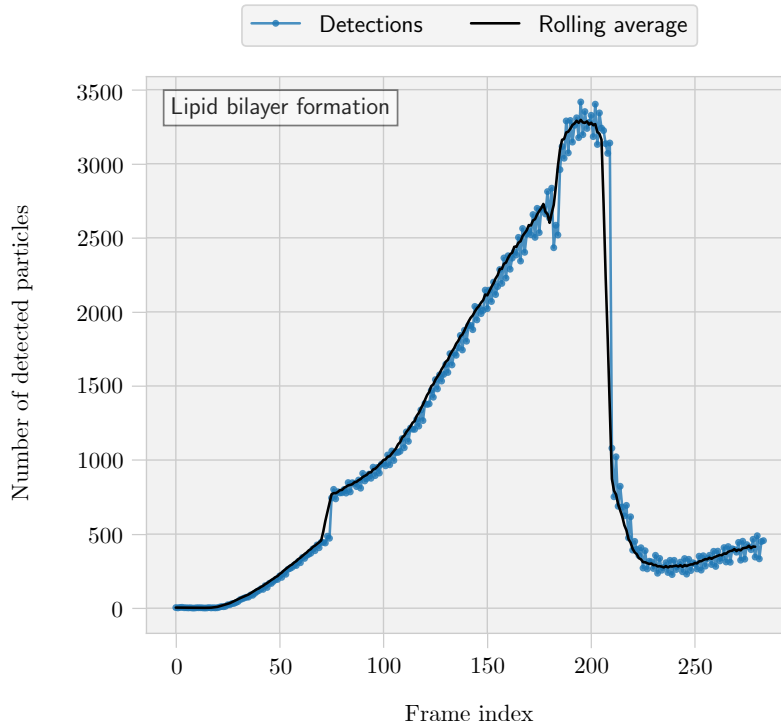


Figure 3: Detected particles per frame while forming the lipid bilayer. Compare this with the number of particles visualized in Figure 2 above. Note the significant drop around frame number ~ 210 , corresponding to case (c) – (d) in Figure 2, which is a consequence of the eruption of the bilayer as explained in the text.

E Experimental Log and Python Code

The experimental log-book that was updated continuously during this project can be found on [GitHub](#). There one can also find the file `analyzer.py`, which was used to process and visualize the data connected to the particle size distributions.